

Copper Nanoparticles with Abundant Defects as a pH-Universal Catalyst for Hydrogen Evolution Reaction

Zi-Zheng Shi, Xueqing Wang, Wen-Jing Kang, Yi-Ming Bai, Jing Yang, Hui Liu, Cun-Ku Dong, Peng-Fei Yin,* and Xi-Wen Du*



Cite This: *ACS Appl. Energy Mater.* 2023, 6, 10012–10019



Read Online

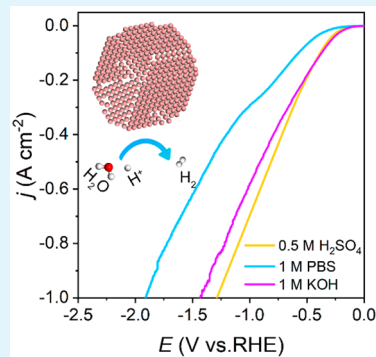
ACCESS |

Metrics & More

Article Recommendations

Supporting Information

ABSTRACT: The development of low-cost, high-activity, and pH universal catalysts is essential in hydrogen evolution reaction (HER) via industrial electrolysis of water. Here, we report the rapid and scalable preparation of defect-rich copper catalysts as electrocatalysts for all-pH HER by electric discharge in liquid (EDL) technology. The defects upshift the d-band center of copper, improve water dissociation and hydrogen adsorption, and ultimately improve the intrinsic catalytic activity. Thus, the overpotentials of Cu catalysts reach 180 mV in 0.5 M H_2SO_4 , 269 mV in 1 M PBS, and 152 mV at 10 mA cm⁻² in 1 M KOH. In addition, the Cu catalysts also exhibit lower overpotentials at high current density (1 A cm⁻²), superior to commercial Pt/C in neutral and alkaline solutions. Our work demonstrates that the EDL is a powerful technique for preparing metallic catalyst, and introducing defects into copper nanoparticles provides a versatile and friendly strategy for improving intrinsic catalytic performance.



KEYWORDS: defects, copper, electrocatalyst, hydrogen evolution reaction, d band center, pH universal

INTRODUCTION

Hydrogen, a green and sustainable energy source, is an effective solution to the growing global energy demand and climate change.^{1,2} In the past decades, the extraction of green hydrogen from renewable energy has become a research hotspot.^{3–5} Among various techniques, the water electrolysis has attracted intensive attention because of the flexible production, high purity and high value oxygen byproduct.^{6–8} The hydrogen production depends closely on the pH value of the electrolyte because the hydrogen evolution reaction (HER) proceeds by different mechanisms under acidic, neutral, and alkaline conditions. Hence, the catalytic performance varies with different pH values, and it is still a challenge to develop HER catalysts that can work efficiently in the full pH range (pH 0–14).^{9,10}

Currently, Pt-based catalysts are the popular catalysts for HER due to their excellent activity.^{11,12} However, the high cost and low reserves of Pt limit its practical applications.^{12–14} By contrast, copper shows extremely low cost, abundant reserves and excellent electrical conductivity, while this catalyst suffers from excessively weak adsorption energy and poor catalytic activity toward HER.^{15,16} Recently, many strategies have been developed to improve the HER activity of Cu-based catalysts, including alloying,^{17,18} morphology control,¹⁹ defect engineering,^{20–22} elemental doping,²³ and surface strain.^{24,25} In particular, defect engineering can modulate the electronic structure and increase the number of active sites, thus improve the intrinsic activity at the atomic level.^{26,27}

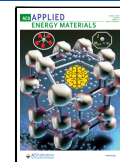
Common techniques for defect engineering include elemental doping,²⁸ chemical etching,²⁹ ion irradiation³⁰ and laser ablation.³¹ For example, Li et al. synthesized Ag nanoparticles by laser ablation of Ag target in liquid, the fast cooling of liquid medium results in the formation of stacking faults and then an excellent HER activity beyond Pt/C.³² Zhao et al. introduced oxygen vacancies into metal oxide catalyst by quenching in salt solution, leading to a significant increase in OER activity.³³ Both works demonstrate that the quenching effect is very effective in generating defects.

Electric discharge in liquid (EDL) is a common process to remove material from the surface of a working piece. When a pulse voltage is applied on two metal electrodes, the liquid medium filled in the electrodes is broken through, leading to the formation of a discharge channel and high temperature plasma (~7000 K).^{34,35} The plasma heats the metal electrodes into vapor or metal droplets which are then quenched into metal nanoparticles by the liquid medium after the electrical pulse.³⁶ Therefore, EDL tends to introduce defects in metal nanoparticles through the quenching effect. In addition, the productivity of EDL can reach 5 g min⁻¹ or even higher, and its

Received: June 28, 2023

Accepted: September 8, 2023

Published: September 20, 2023



Scheme 1. Schematic Description on the Synthesis of E-Cu. (a) The EDL Device and Working State. (b) The Formation of Copper Droplets and Vapor during the Discharge Pulse. (c) The Formation of E-Cu Nanoparticles by Rapid Quenching

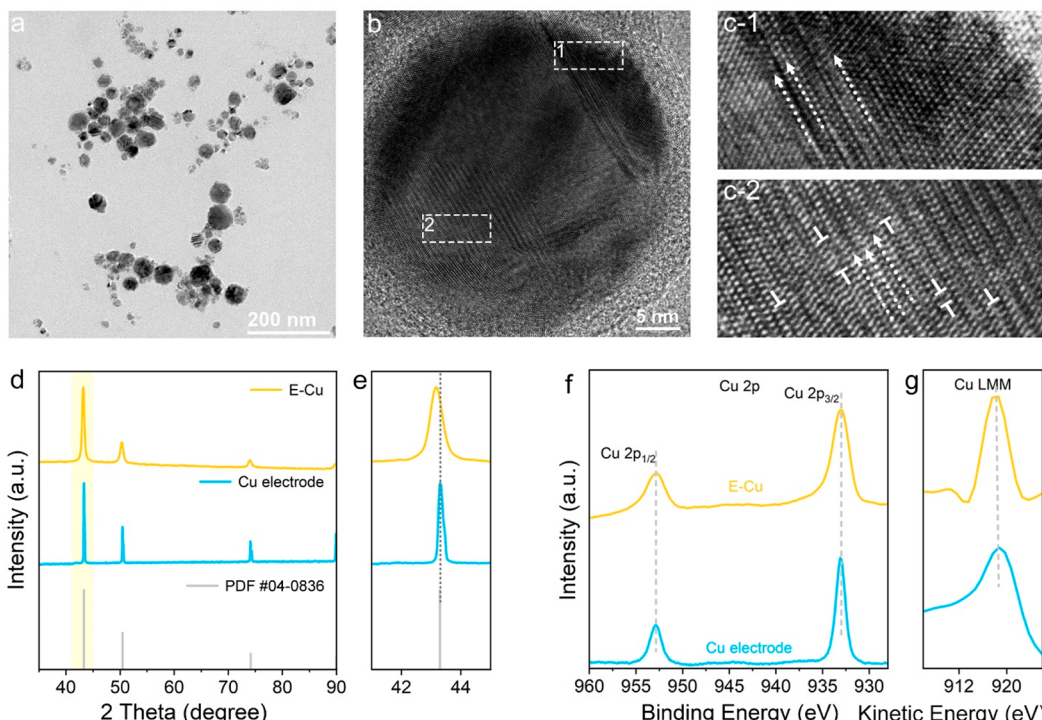
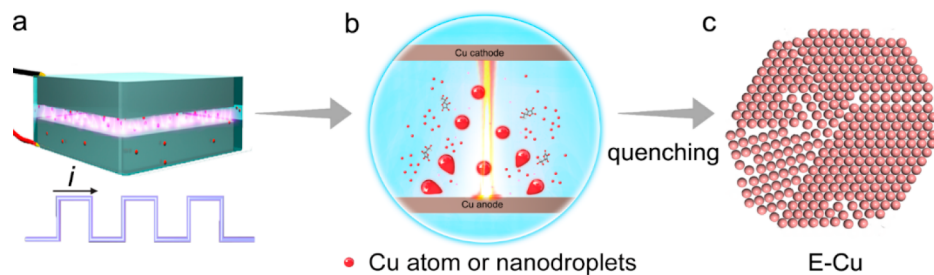


Figure 1. Characterization of E-Cu nanoparticles. (a) Low-resolution TEM image. (b) High-resolution TEM images. (c) Enlarged images in the frames in panel b. (d) XRD pattern. (e) An enlarged image corresponding to the yellow marked area in (d). (f) Cu 2p XPS spectrum. (g) Cu AES spectrum. The white \perp symbols represent the dislocations, and the white dotted arrows represent stacking faults.

high efficiency, convenience, nonpollution will be beneficial for industrial applications.

In this work, we report the preparation of Cu nanoparticles enriched with dislocations and stacking faults by EDL for catalyzing the HER in the full pH range. The defects change the local electronic structure, enhance the d-band center, and improve the intrinsic activity of the Cu nanoparticles. As a result, defect-rich Cu nanoparticles exhibit excellent HER under acidic, neutral, and basic conditions. The overpotentials at 10 mA cm^{-2} were 180 mV (acidic), 269 mV (neutral), and 152 mV (basic), which are much better than those of defect-free Cu nanoparticles. Meanwhile, the defect-rich Cu nanoparticles exhibit excellent stability, maintaining excellent performance after 50 h of operation at 200 mA cm^{-2} . Our work demonstrates that EDL is a powerful technique to generate defects in Cu nanoparticles, which provides an effective solution to enhance the HER activity of inexpensive metal catalysts.

RESULTS AND DISCUSSION

Scheme 1 shows the EDL process for the preparation of defect-rich copper nanoparticles (E-Cu). In a typical experiment, two copper rods were immersed in aqueous ascorbic acid solution (10 mmol L^{-1}) and used as the cathode and anode, respectively (Figure S1a). A pulsed voltage (70 V) is applied on the electrodes (Scheme 1a), and during the discharge pulse, a high-energy plasma bombs the Cu electrode to produce a large number of copper droplets or copper vapor (Scheme 1b). During the pulse interval, the quenching effect of the surrounding liquid cools the copper droplets and retains the disordered structure formed at high temperature (Scheme 1c). In addition, the reductive ascorbic acid in the solution can prevent the copper nanoparticles from oxidation. As such, bulk copper was successfully transformed into copper nanoparticles with abundant defects (Figure S1b). For comparison, E-Cu sample was annealed to obtain a so-called A-Cu sample with a lower defect density (Figures S6–S8), and defect-free nanoparticles with similar particle size to E-Cu were

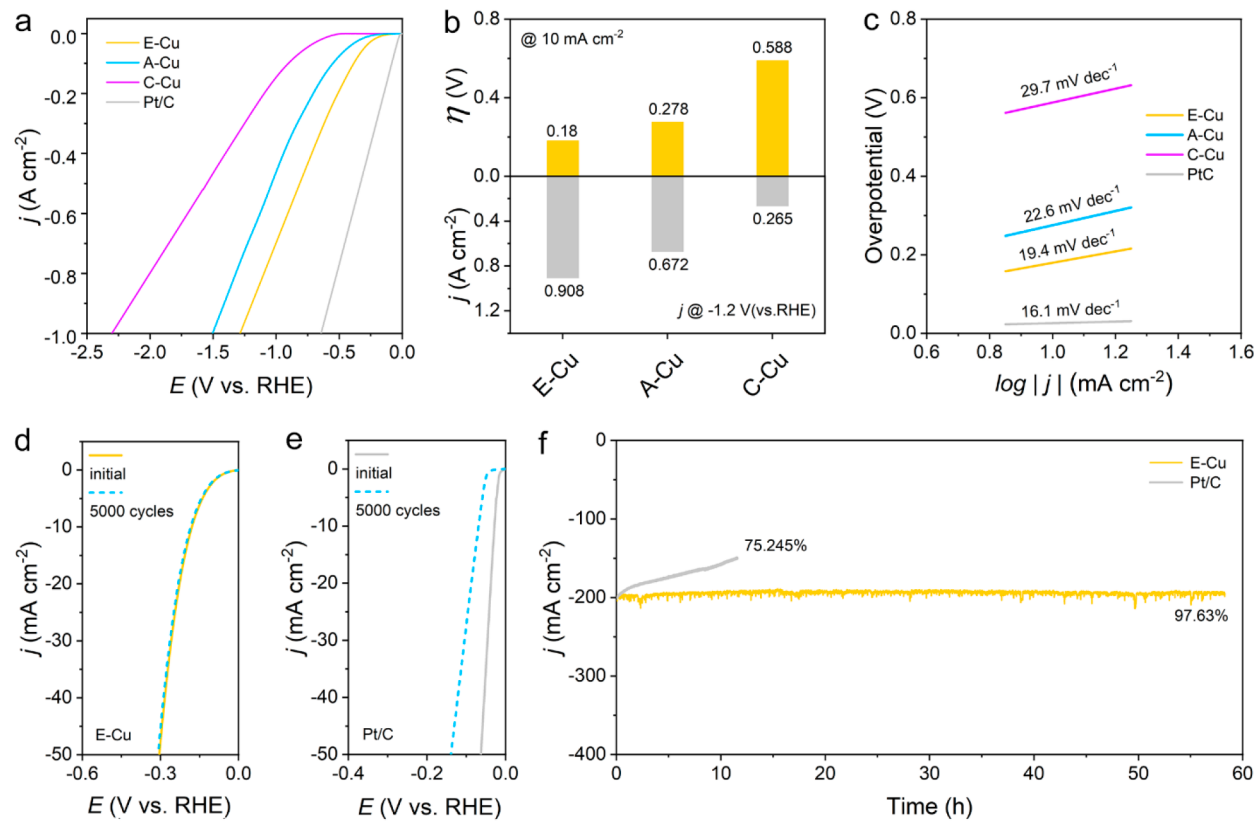


Figure 2. HER performance of different catalysts in 0.5 M H_2SO_4 electrolyte. (a) LSV curves of E-Cu, A-Cu, C-Cu and Pt/C. (b) Overpotentials at 10 mA cm^{-2} and current densities at -1.2 V vs RHE of E-Cu, A-Cu and C-Cu. (c) Tafel slope plots based on LSV curves in panel a. (d) E-Cu and (e) Pt/C LSV curves before and after 5000 CV cycles. (f) Current–time (i – t) lines of E-Cu and Pt/C at an applied voltage of -0.55 V vs RHE.

synthesized by a chemical method reported in the literature³⁷ and denoted as C–Cu (Figures S9 and S10).

Figure 1a shows the transmission electron microscope (TEM) image of E-Cu, which contains nanoparticles with sizes of $23.5 \pm 3 \text{ nm}$ (Figure S2). High-resolution TEM (HRTEM) images reveal that E-Cu contains irregular lattices (Figure 1b). The enlarged view of the selected areas in Figure 1b indicates that there are abundant stacking faults and edge dislocations in E-Cu (Figure 1c). Figures S4 and S5 indicate that the other particles also contain a large number of defects. X-ray diffraction (XRD, Figures 1d, 1e), X-ray photoelectron spectroscopy (XPS, Figure 1f) and Auger electron spectroscopy (AES, Figure 1g) jointly manifest that the synthesized copper nanoparticles were free from oxidation. In addition, the XRD peaks of E-Cu shift slightly to the left side compared with bulk Cu, and the fitting result suggests a weak tensile strain (0.9%), which is consistent with the planar spacing of 2.16 nm measured in the TEM image (Figure S3).

To investigate the influence of defects on the HER activity, we perform electrochemical tests in a standard three-electrode system calibrated by a reversible hydrogen electrode (RHE, Figure S11). First, we compared the performance of E-Cu, A-Cu, and C–Cu in acidic media ($0.5 \text{ M } \text{H}_2\text{SO}_4$, $\text{pH} \approx 0$) (Figures 2, S12). As shown in the linear scanning voltammetry (LSV) curves without iR -correction (Figure 2a), an overpotential of 180 mV @ 10 mA cm^{-2} was achieved by E-Cu, much better than 275 mV of A-Cu and 588 mV of C–Cu (Figure 2b), obviously, the overpotential decreases with the rise of the defect density. Moreover, the current density can

reach 0.908 A cm^{-2} at an overpotential of 1.2 V vs RHE, and after iR -correction, the overpotential is only 0.783 V vs RHE at a current density of 1 A cm^{-2} (Figure 2). The Tafel plots were derived from LSV curves and are shown in Figure 2c, and the values for E-Cu, A-Cu, C–Cu, and Pt/C are 19.4 , 22.6 , 29.7 , and 16.1 mV dec^{-1} , respectively. The Tafel slope of E-Cu study indicates that HER occurs on this catalyst through a Volmer–Tafel mechanism, namely, H–H bond formation through direct Tafel coupling as the rate-determining step. The exchange current density (j_0) for each sample was obtained by extrapolation of the corresponding Tafel slope (Figure S13). The j_0 for E-Cu ($\sim 0.723 \text{ mA cm}^{-2}$) is higher than that of C–Cu (0.594 mA cm^{-2}). The electrochemical active surface area (ECSA) of the catalyst was evaluated by electrochemical double layer capacitance (Figure S14). Also, the value of E-Cu (12.02 mF cm^{-2}) is much larger than that of C–Cu (5.19 mF cm^{-2}) (Figure S14). In addition, E-Cu still showed the highest HER activity after normalization of the LSV curve with the ECSA (Figure S15). The above results indicate that the introduction of defects into Cu nanoparticles exposes more electrochemical active sites as well as increases the intrinsic activity of the active sites.

Moreover, E-Cu exhibits the smallest semicircle in the Nyquist plot of electrochemical impedance spectroscopy (EIS) analysis (Figure S16), indicating the lowest charge transfer resistance ($R_{ct} = 17.22 \Omega$) between the catalyst and the electrolyte interface. Long-term stability is another critical indicator for electrocatalysts; E-Cu showed almost no change in overpotential and Tafel slope after 5000 cycles of CV

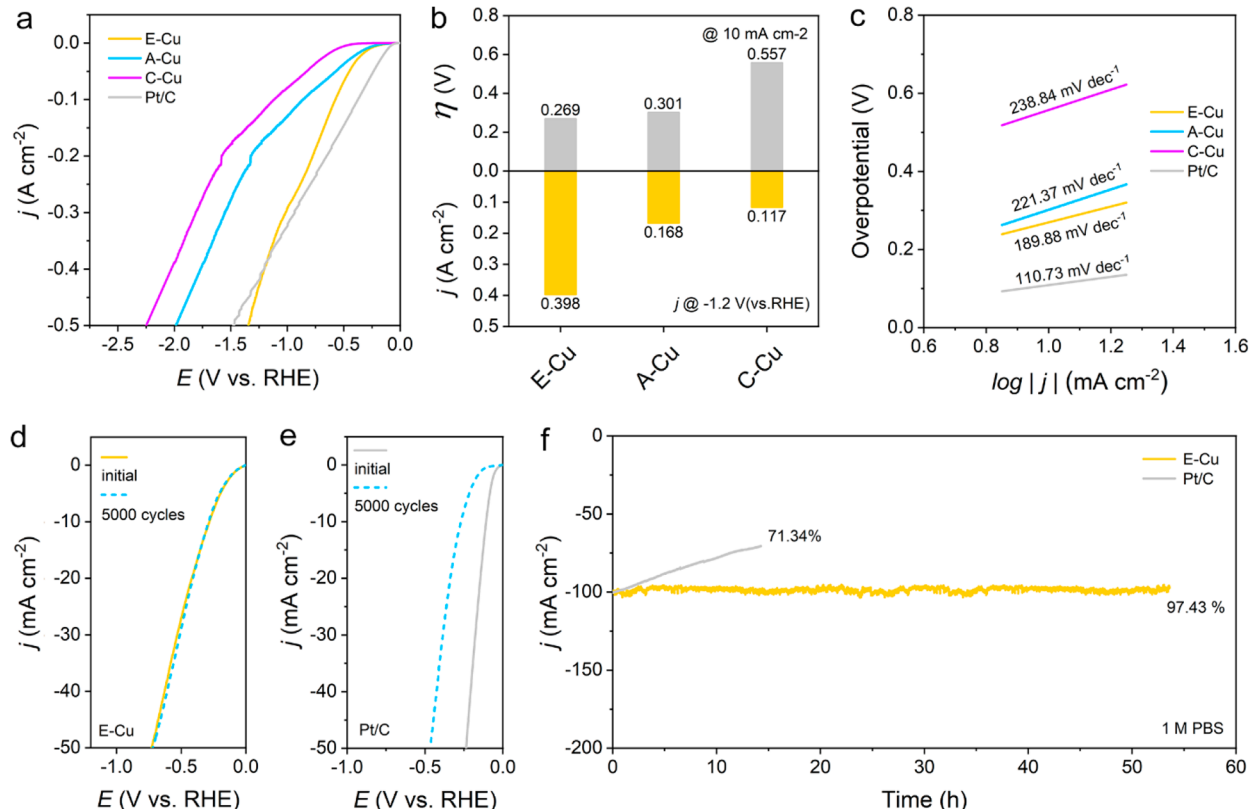


Figure 3. HER performance of different catalysts in 1 M PBS electrolyte. (a) LSV curves of E-Cu, A-Cu, C-Cu and Pt/C. (b) Overpotentials at 10 mA cm^{-2} and current densities at -1.2 V vs RHE of E-Cu, A-Cu and C-Cu. (c) Tafel slope plots based on LSV curves in panel a. (d) E-Cu and (e) Pt/C LSV curves before and after 5000 CV cycles. (f) Current–time ($i-t$) lines of E-Cu and Pt/C at an applied voltage of -0.6 V vs RHE.

stability testing (Figure 2d), while the overpotential of commercial Pt/C became significantly higher by tens of millivolts (Figure 2e). Furthermore, at a high overpotential of -0.52 V vs RHE, E-Cu can operate stably for $\geq 55 \text{ h}$ continuously with only a slight decay (Figure 2f).

Although HER proceeds easily under acidic conditions, the acid electrolyte corrodes the electrolyzer and catalyst and shortens their life. By contrast, a neutral medium provides a more safe circumstance for the device. We then tested E-Cu in an Ar-saturated 1 M PBS solution at pH 7.0. As shown in Figures 3a,b and S17, E-Cu exhibited an overpotential of 269 mV at 10 mA cm^{-2} , lower than A-Cu (302 mV) and C-Cu (557 mV). Particularly, the overpotential of E-Cu was even lower than that of commercial Pt/C when the current density exceeded 0.383 A cm^{-2} (Figure S17). In comparison with the other samples, E-Cu exhibits a lower Tafel slope ($143.58 \text{ mV dec}^{-1}$) and higher exchange current density (0.446 mA cm^{-2}) (Figures 3c and S18), suggesting the higher reaction kinetics on E-Cu under neutral conditions. The superior neutral HER activity of E-Cu is attributed to its high specific surface area ECSA ($C_{\text{dl}} = 13.4 \text{ mF cm}^{-2}$, Figure S19), high intrinsic activity ($j_{\text{ECSA}} = 2.8 \text{ mA cm}^{-2}$ at 1 V vs RHE, Figure S20) and faster charge transfer R_{ct} (24.44Ω , Figure S21). In addition, the activity of E-Cu remains essentially unchanged after 5000 cycles (Figure 3d,e), and remains stable for more than 55 h at a high working potential (Figure 3f).

Industrial water electrolysis tends to take place in alkaline electrolytes due to mild working conditions. In addition, alkaline HER is a key step in the chlor-alkali process, which is an energy intensive practice.³⁸ However, the HER in alkaline

solutions has relatively slow kinetics compared to acidic solutions and therefore requires a high overpotential to drive the reaction. Therefore, the design and preparation of high-performance HER catalysts for alkaline media are crucial to reducing energy consumption. Next, we evaluated the alkaline HER activity of E-Cu in Ar-saturated 1 M KOH. As shown in Figures 4a,b and S21, the overpotential of E-Cu was 152 mV at 10 mA cm^{-2} , superior to that of A-Cu (239 mV), and C-Cu (519 mV). In particular, at a current density of 1 A cm^{-2} , the overpotential of E-Cu (1.433 V) is much better than that of commercial Pt/C (Figure S22). Furthermore, E-Cu possesses the lowest Tafel slope ($136.54 \text{ mV dec}^{-1}$; Figure 4c), the largest exchange current density (0.716 mA cm^{-2} , Figure S23), the largest C_{dl} value (13.56 mF cm^{-2} ; Figure S24) and the smallest R_{ct} (10.6Ω , Figure S26). The LSV plots normalized by ECSA are shown in Figure S25, with E-Cu showing the highest specific activity. Based on the above, we can conclude that more active sites with higher intrinsic activity and better charge transfer efficiency contribute to the excellent alkaline HER performance of E-Cu. In addition, E-Cu shows a good stability, the LSV curves before and after 5000 CV cycles almost overlap (Figure 4d), and the working current (200 mA cm^{-2}) does not decay after 63 h of continuous testing (Figure 4f). This means that E-Cu has the potential for practical application regarding its low overpotential and good stability.³⁹

We further investigated the changes in structure and valence of the E-Cu after the stability testing in acidic, neutral, and alkaline solution. Referring to Figure S27, the TEM images and the corresponding particle size distributions indicate that the particle size remains unchanged. A high density of defects can

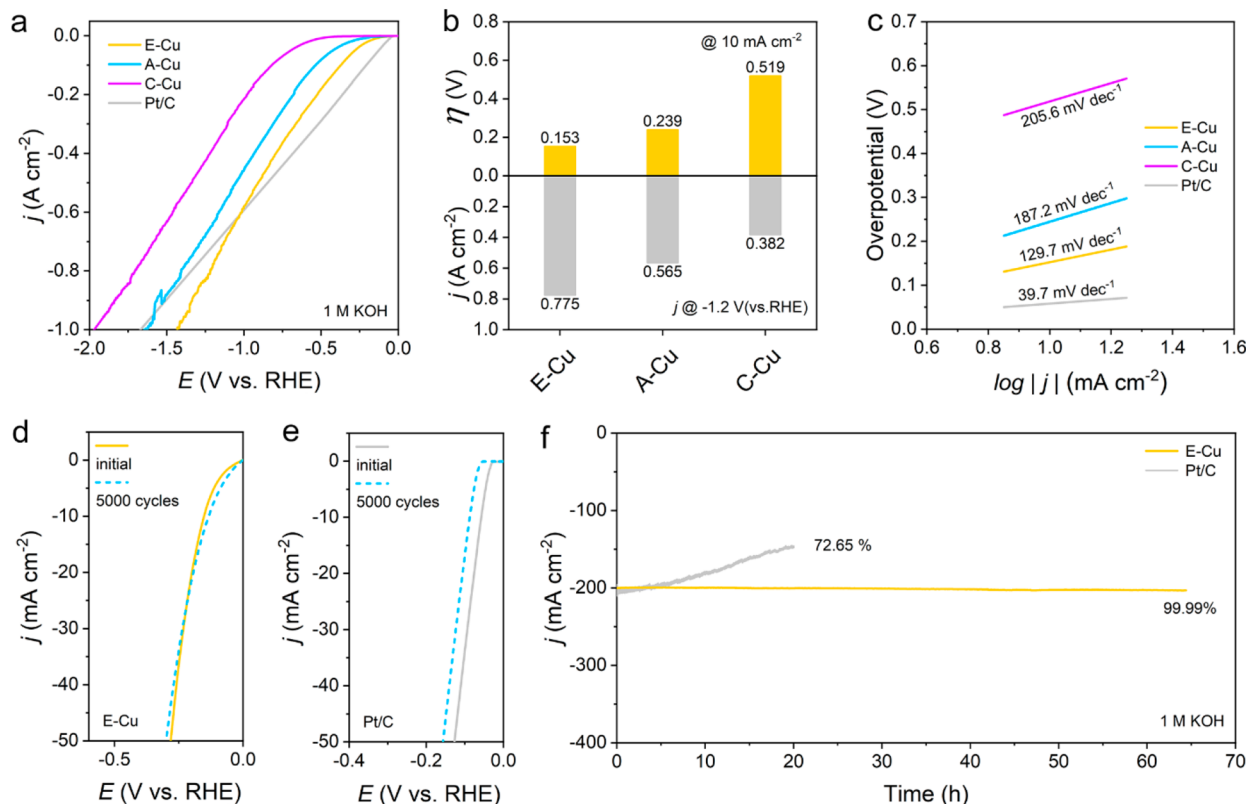


Figure 4. HER performance of different catalysts in an electrolyte saturated with 1 M KOH under Ar. (a) LSV curves without iR -correction of E-Cu, A-Cu, C-Cu and Pt/C. (b) Relationship between overpotential at 10 mA cm^{-2} and current density at -1.2 V vs RHE. (c) Tafel slope plots based on LSV curves in panel a. (d) E-Cu and (e) Pt/C LSV curves before and after 5000 CV cycles. (f) Current–time (i – t) lines of E-Cu and Pt/C at an applied voltage of -0.53 V vs RHE.

still be observed in the HRTEM images (Figures S28–S30). XPS spectra of the E-Cu show a metallic state (Figure S31), and the inductively coupled plasma mass spectrometry (ICP-MS) measurement of the electrolyte (Table S1) indicates there is no dissolution of Cu during the HER. The above results jointly confirm the structural and chemical stability of E-Cu.

To further explore the influence of defects on Cu nanoparticles, the defect density on the surfaces was evaluated by the ratio of Q_{defects}/Q (Figures 5a, S36), where Q_{defects} is the charge intensity of reversible O-adsorption peak ($>0.3 \text{ V}$, which is strongly correlated with surface defects⁴⁰), and Q is the charge due to the Cu crystal surface ($-0.25 \sim -0.05 \text{ V}$ vs RHE, which is attributed to the reversible $^{*}\text{OH}$ adsorption, see Supporting Information for more details).^{41–43} As shown in Figure 5b, the HER exchange current density increases with the defect density, while the charge transfer resistance decreases with the defect density. These results manifest that the highly dense defects promote the catalytic activity and accelerate the reduction reaction at the solid/liquid interface.

Next, we explore the influence of the defect on the d-band center. We collected XPS valence band spectra to fit the d-band center of different copper catalysts, as shown in Figure 5c,d, the d-band center of Cu increased significantly with increasing defect density, the d-band center of E-Cu (-2.44 eV) is much higher than that of C-Cu (-3.19 eV), suggesting the defects in E-Cu enhance the d-band center remarkably, which is because defects can reduce the coordination number of Cu and produce weak tensile strains.³²

Based on the above, the high catalytic performance of E-Cu can be rationalized as below: Acidic HER involves hydrogen

adsorption and dissociation, whereas basic and neutral HER processes involve more reactive steps such as water adsorption and dissociation. Copper metal possesses the fully occupied d-orbitals and low d-band center,⁴⁴ after the H or OH radicals adsorb to the copper surface, the antibonding molecular orbitals are lower than the Fermi level, leading to capability.⁴⁵ The defects in copper catalysts can improve the catalytic properties in three aspects: First, the defect can elevate the d-band center, increase the occupation of antibonding orbitals, and enhance the adsorptive capability and then the intrinsic catalytic activity (Figure S37). Second, the defects enlarge the electrochemically active surface area, providing more active sites for promoting HER processes. Third, Cu possess a low formation energy for stacking fault;⁴⁶ the defects in E-Cu are relatively stable, so the existence of defects will not lead to significant attenuation of stability compared to the A-Cu (with defects; more details, see Figures S32–S35).

CONCLUSION

We adopted an electric discharge machining process to rapidly prepare large quantities of defect-rich copper catalysts. The catalyst shows high all-pH catalytic activity toward HER than chemically synthesized defect-free copper nanoparticles and even outperformed commercial Pt/C current densities at high working potentials. In addition, the catalyst exhibits long-term stability as well as excellent corrosion resistance. The superior HER performance is attributed to the high-density defects which improve the d-band center and then overcome the weak adsorption of the copper catalyst. This work demonstrates that

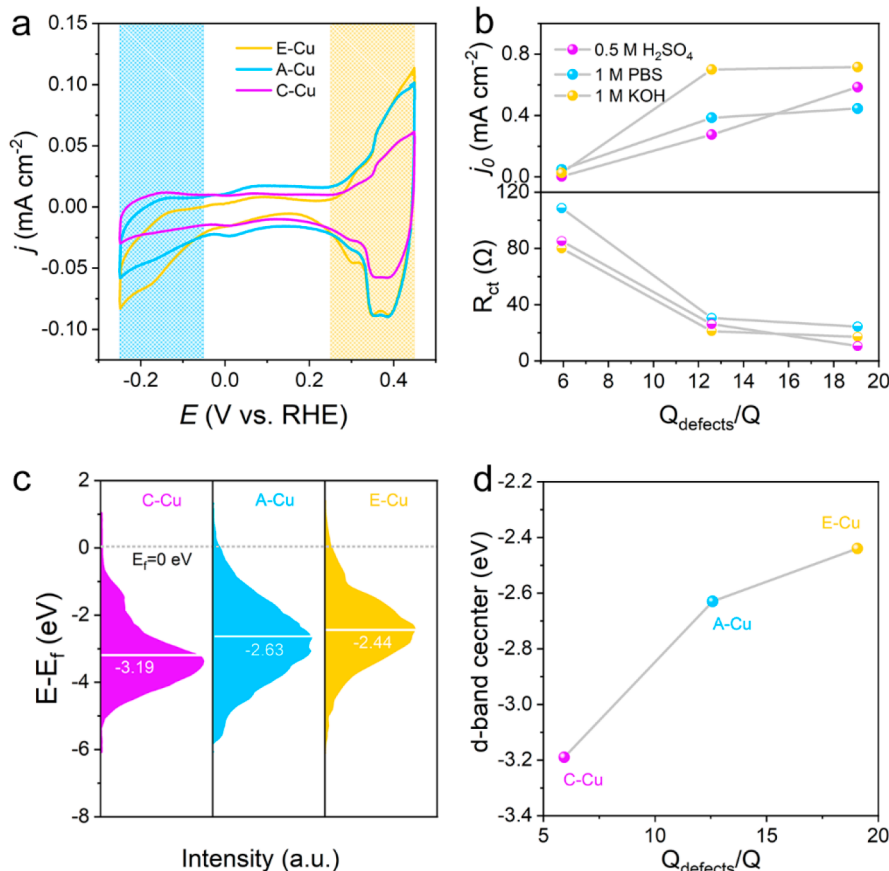


Figure 5. Defect density and electronic structure relationships for catalysts. (a) Cyclic voltammetry curves recorded in 0.1 M NaOH at 50 mV s^{-1} for E-Cu, A-Cu and C-Cu. Features corresponding to Cu surface are shaded in blue, while those corresponding to defects are highlighted in orange. (b) Relationship between defect density and exchange current density (j_0) (upper figure), and the relationship between defect density and charge transfer resistance (R_{ct}) (bottom figure). (c) XPS valence band spectra and the fitted d-band center. (d) Relationship between defect density and the d-band center.

electric discharge is powerful in producing abundant defects, which can endow inactive metallic catalysts with high catalytic performance.

ASSOCIATED CONTENT

Supporting Information

The Supporting Information is available free of charge at <https://pubs.acs.org/doi/10.1021/acsaem.3c01611>.

Methods for preparation, characterization, and electrochemical testing; optical photographs, HRTEM and IFFT images of E-Cu; TEM, XRD, XPS and LMM spectra of A-Cu, C-Cu and after long-term HER testing in 1 M KOH; ICP-MS measurement of Cu in the electrolyte before and after the HER durability test of E-Cu; exchange current density, electrochemically active area, normalized current density and EIS at different pH (PDF)

AUTHOR INFORMATION

Corresponding Authors

Peng-Fei Yin – School of Materials Science and Engineering, Tianjin University, Tianjin 300350, China;
Email: pengfeiyin@tju.edu.cn
Xi-Wen Du – School of Materials Science and Engineering, Tianjin University, Tianjin 300350, China; orcid.org/0000-0002-2811-147X; Email: xwdu@tju.edu.cn

Authors

Zi-Zheng Shi – School of Materials Science and Engineering, Tianjin University, Tianjin 300350, China
Xueqing Wang – School of Materials Science and Engineering, Tianjin University, Tianjin 300350, China
Wen-Jing Kang – School of Materials Science and Engineering, Tianjin University, Tianjin 300350, China
Yi-Ming Bai – School of Materials Science and Engineering, Tianjin University, Tianjin 300350, China; orcid.org/0000-0002-2920-0386
Jing Yang – School of Materials Science and Engineering, Tianjin University, Tianjin 300350, China; orcid.org/0000-0002-3731-368X
Hui Liu – School of Materials Science and Engineering, Tianjin University, Tianjin 300350, China; orcid.org/0000-0001-8183-9446
Cun-Ku Dong – School of Materials Science and Engineering, Tianjin University, Tianjin 300350, China; orcid.org/0000-0001-8277-6707

Complete contact information is available at: <https://pubs.acs.org/10.1021/acsaem.3c01611>

Author Contributions

X.-W.D. and P.-F.Y. designed the project. Z.-Z.S. and X.W. performed the experiment under the direction of X.-W.D. Z.-Z.S. performed the experimental data analysis. Z.-Z.S., P.-F.Y.

and X.-W.D. wrote the paper. All authors discussed the results and commented on the manuscript.

Notes

The authors declare no competing financial interest.

ACKNOWLEDGMENTS

This work is supported by the National Natural Science Foundation of China (NSFC) (grant nos. 52373302, 52101266 and 51871160) and the Natural Science Foundation of Hefei (grant no. 2022046).

ABBREVIATIONS

CCR2, CC chemokine receptor 2; CCL2, CC chemokine ligand 2; CCR5, CC chemokine receptor 5; TLC, thin layer chromatography

REFERENCES

- (1) Zhu, Y. P.; Guo, C.; Zheng, Y.; Qiao, S.-Z. Surface and Interface Engineering of Noble-Metal-Free Electrocatalysts for Efficient Energy Conversion Processes. *Acc. Chem. Res.* **2017**, *50* (4), 915–923.
- (2) Ge, Y.; Wang, X.; Chen, B.; Huang, Z.; Shi, Z.; Huang, B.; Liu, J.; Wang, G.; Chen, Y.; Li, L.; Lu, S.; Luo, Q.; Yun, Q.; Zhang, H. Preparation of fcc-2H-fcc Heterophase Pd@Ir Nanostructures for High-Performance Electrochemical Hydrogen Evolution. *Adv. Mater.* **2022**, *34* (4), 2107399.
- (3) Wang, S.; Lu, A. L.; Zhong, C. J. Hydrogen production from water electrolysis: role of catalysts. *Nano Converg.* **2021**, *8* (1), 4.
- (4) Yan, Y.; Xia, B. Y.; Zhao, B.; Wang, X. A review on noble-metal-free bifunctional heterogeneous catalysts for overall electrochemical water splitting. *J. Mater. Chem.* **2016**, *4* (45), 17587–17603.
- (5) Liu, F.; Shi, C. X.; Guo, X. L.; He, Z. X.; Pan, L.; Huang, Z. F.; Zhang, X. W.; Zou, J. J. Rational Design of Better Hydrogen Evolution Electrocatalysts for Water Splitting: A Review. *Adv. Sci.* **2022**, *9* (18), 2200307.
- (6) Yu, Z. Y.; Duan, Y.; Feng, X. Y.; Yu, X. X.; Gao, M. R.; Yu, S. H. Clean and Affordable Hydrogen Fuel from Alkaline Water Splitting: Past, Recent Progress, and Future Prospects. *Adv. Mater.* **2021**, *33* (31), 2007100.
- (7) Yu, P.; Wang, F. M.; Shifa, T. A.; Zhan, X. Y.; Lou, X. D.; Xia, F.; He, J. Earth abundant materials beyond transition metal dichalcogenides: A focus on electrocatalyzing hydrogen evolution reaction. *Nano Energy* **2019**, *58*, 244–276.
- (8) Li, M.; Zhu, H.; Yuan, Q.; Li, T.; Wang, M.; Zhang, P.; Zhao, Y.; Qin, D.; Guo, W.; Liu, B.; Yang, X.; Liu, Y.; Pan, Y. Proximity Electronic Effect of Ni/Co Diatomic Sites for Synergistic Promotion of Electrocatalytic Oxygen Reduction and Hydrogen Evolution. *Adv. Funct. Mater.* **2023**, *33* (4), 2210867.
- (9) Tian, X. Y.; Zhao, P. C.; Sheng, W. C. Hydrogen Evolution and Oxidation: Mechanistic Studies and Material Advances. *Adv. Mater.* **2019**, *31* (31), 1808066.
- (10) Mahmood, N.; Yao, Y. D.; Zhang, J. W.; Pan, L.; Zhang, X. W.; Zou, J. J. Electrocatalysts for Hydrogen Evolution in Alkaline Electrolytes: Mechanisms, Challenges, and Prospective Solutions. *Adv. Sci.* **2018**, *5* (2), 1700464.
- (11) Dai, J.; Zhu, Y. L.; Chen, Y.; Wen, X.; Long, M. C.; Wu, X. H.; Hu, Z. W.; Guan, D. Q.; Wang, X. X.; Zhou, C.; Lin, Q.; Sun, Y.; Weng, S.; Wang, H.; Zhou, W.; Shao, Z. Hydrogen spillover in complex oxide multifunctional sites improves acidic hydrogen evolution electrocatalysis. *Nat. Commun.* **2022**, *13* (1), 1189.
- (12) Ledezma-Yanez, I.; Wallace, W. D. Z.; Sebastian-Pascual, P.; Climent, V.; Feliu, J. M.; Koper, M. T. M. Interfacial water reorganization as a pH-dependent descriptor of the hydrogen evolution rate on platinum electrodes. *Nat. Energy* **2017**, *2* (4), 17031.
- (13) Wang, P. T.; Jiang, K. Z.; Wang, G. M.; Yao, J. L.; Huang, X. Q. Phase and Interface Engineering of Platinum-Nickel Nanowires for Efficient Electrochemical Hydrogen Evolution. *Angew. Chem., Int. Ed.* **2016**, *55* (41), 12859–12863.
- (14) Wang, M.; Sun, K.; Mi, W.; Feng, C.; Guan, Z.; Liu, Y.; Pan, Y. Interfacial Water Activation by Single-Atom Co-N₃ Sites Coupled with Encapsulated Co Nanocrystals for Accelerating Electrocatalytic Hydrogen Evolution. *ACS Catal.* **2022**, *12* (17), 10771–10780.
- (15) Lu, Q.; Hutchings, G. S.; Yu, W. T.; Zhou, Y.; Forest, R. V.; Tao, R. Z.; Rosen, J.; Yonemoto, B. T.; Cao, Z. Y.; Zheng, H. M.; Xiao, J. Q.; Jiao, F.; Chen, J. G. G. Highly porous non-precious bimetallic electrocatalysts for efficient hydrogen evolution. *Nat. Commun.* **2015**, *6*, 66567.
- (16) Kannimuthu, K.; Sangeetha, K.; Sam Sankar, S.; Karmakar, A.; Madhu, R.; Kundu, S. Investigation on nanostructured Cu-based electrocatalysts for improvising water splitting: a review. *Inorg. Chem. Front.* **2021**, *8* (1), 234–272.
- (17) Shi, H.; Zhou, Y.-T.; Yao, R.-Q.; Wan, W.-B.; Zhang, Q.-H.; Gu, L.; Wen, Z.; Lang, X.-Y.; Jiang, Q. Intermetallic Cu₅Zr Clusters Anchored on Hierarchical Nanoporous Copper as Efficient Catalysts for Hydrogen Evolution Reaction. *Research* **2020**, *2020*, 2987234.
- (18) Ahsan, M. A.; Puente Santiago, A. R.; Hong, Y.; Zhang, N.; Cano, M.; Rodriguez-Castellon, E.; Echegoyen, L.; Sreenivasan, S. T.; Noveron, J. C. Tuning of Trifunctional NiCu Bimetallic Nanoparticles Confined in a Porous Carbon Network with Surface Composition and Local Structural Distortions for the Electrocatalytic Oxygen Reduction, Oxygen and Hydrogen Evolution Reactions. *J. Am. Chem. Soc.* **2020**, *142* (34), 14688–14701.
- (19) Raaijman, S. J.; Arulmozhi, N.; Koper, M. T. M. Morphological Stability of Copper Surfaces under Reducing Conditions. *ACS Appl. Mater. Interfaces* **2021**, *13* (41), 48730–48744.
- (20) Zhuang, P.; Sun, Y.; Dong, P.; Smith, W.; Sun, Z.; Ge, Y.; Pei, Y.; Cao, Z.; Ajayan, P. M.; Shen, J.; Ye, M. Revisiting the Role of Active Sites for Hydrogen Evolution Reaction through Precise Defect Adjusting. *Adv. Funct. Mater.* **2019**, *29* (33), 1901290.
- (21) Dey, A.; Chandrabose, G.; Damptey, L. A. O.; Erakulan, E. S.; Thapa, R.; Zhuk, S.; Dalapati, G. K.; Ramakrishna, S.; Braithwaite, N. S. J.; Shirzadi, A.; Krishnamurthy, S. Cu₂O/CuO heterojunction catalysts through atmospheric pressure plasma induced defect passivation. *Appl. Surf. Sci.* **2021**, *541*, 148571.
- (22) Huang, C.-L.; Sasaki, K.; Senthil Raja, D.; Hsieh, C.-T.; Wu, Y.-J.; Su, J.-T.; Cheng, C.-C.; Cheng, P.-Y.; Lin, S.-H.; Choi, Y.; Lu, S. Y. Twinning Enhances Efficiencies of Metallic Catalysts toward Electrolytic Water Splitting. *Adv. Energy Mater.* **2021**, *11* (46), 2101827.
- (23) Zhang, L.; Gao, X. R.; Zhu, Y.; Liu, A.; Dong, H. L.; Wu, D. J.; Han, Z. D.; Wang, W.; Fang, Y.; Zhang, J.; Kou, Z.; Qian, B.; Wang, T. T. Electrocatalytically inactive copper improves the water adsorption/dissociation on Ni₃S₂ for accelerated alkaline and neutral hydrogen evolution. *Nanoscale* **2021**, *13* (4), 2456–2464.
- (24) Kang, W. J.; Feng, Y.; Li, Z.; Yang, W. Q.; Cheng, C. Q.; Shi, Z. Z.; Yin, P. F.; Shen, G. R.; Yang, J.; Dong, C. K.; Liu, H.; Ye, F. X.; Du, X. W. Strain-Activated Copper Catalyst for pH-Universal Hydrogen Evolution Reaction. *Adv. Funct. Mater.* **2022**, *32* (18), 2112367.
- (25) Wang, Z. D.; Zang, Y.; Liu, Z. J.; Peng, P.; Wang, R.; Zang, S. Q. Opening catalytic sites in the copper-triazoles framework via defect chemistry for switching on the proton reduction. *Appl. Catal., B* **2021**, *288*, 119941.
- (26) Lei, Y. P.; Wang, Y. C.; Liu, Y.; Song, C. Y.; Li, Q.; Wang, D. S.; Li, Y. D. Designing Atomic Active Centers for Hydrogen Evolution Electrocatalysts. *Angew. Chem., Int. Ed.* **2020**, *59* (47), 20794–20812.
- (27) Wu, T.; Dong, C. L.; Sun, D.; Huang, F. Q. Enhancing electrocatalytic water splitting by surface defect engineering in two-dimensional electrocatalysts. *Nanoscale* **2021**, *13* (3), 1581–1595.
- (28) Zhang, J. J.; Zhang, C. H.; Wang, Z. Y.; Zhu, J.; Wen, Z. W.; Zhao, X. Z.; Zhang, X. X.; Xu, J.; Lu, Z. G. Synergistic Interlayer and Defect Engineering in VS₂ Nanosheets toward Efficient Electrocatalytic Hydrogen Evolution Reaction. *Small* **2018**, *14* (9), 1703098.
- (29) Liu, D. L.; Wang, C. H.; Yu, Y. F.; Zhao, B. H.; Wang, W. C.; Du, Y. H.; Zhang, B. Understanding the Nature of Ammonia Treatment to Synthesize Oxygen Vacancy-Enriched Transition Metal Oxides. *Chem.* **2019**, *5* (2), 376–389.

- (30) Zhang, Y. Q.; Rawat, R. S.; Fan, H. J. Plasma for Rapid Conversion Reactions and Surface Modification of Electrode Materials. *Small Methods* 2017, 1 (9), 1700164.
- (31) Zhang, Y.; Tao, L.; Xie, C.; Wang, D.; Zou, Y.; Chen, R.; Wang, Y.; Jia, C.; Wang, S. Defect Engineering on Electrode Materials for Rechargeable Batteries. *Adv. Mater.* 2020, 32 (7), 1905923.
- (32) Li, Z.; Fu, J.-Y.; Feng, Y.; Dong, C.-K.; Liu, H.; Du, X.-W. A silver catalyst activated by stacking faults for the hydrogen evolution reaction. *Nat. Catal.* 2019, 2 (12), 1107–1114.
- (33) Ye, C.; Liu, J.; Zhang, Q.; Jin, X.; Zhao, Y.; Pan, Z.; Chen, G.; Qiu, Y.; Ye, D.; Gu, L.; Waterhouse, G. I. N.; Guo, L.; Yang, S. H. Activating Metal Oxides Nanocatalysts for Electrocatalytic Water Oxidation by Quenching-Induced Near-Surface Metal Atom Functionality. *J. Am. Chem. Soc.* 2021, 143 (35), 14169–14177.
- (34) Guo, J.; Mu, X.; Song, S.; Ren, Y.; Wang, K.; Lu, Z. Preparation of Ag⁰ Nanoparticles by EDM Method as Catalysts for Oxygen Reduction. *Metals* 2021, 11 (9), 1491.
- (35) Niu, S.; Yang, Z.; Qi, F.; Han, Y.; Shi, Z.; Qiu, Q.; Han, X.; Wang, Y.; Du, X. Electrical Discharge Induced Bulk-to-Nanoparticle Transformation: Nano High-Entropy Carbide as Catalysts for Hydrogen Evolution Reaction. *Adv. Funct. Mater.* 2022, 32 (35), 2203787.
- (36) Saito, G.; Akiyama, T. Nanomaterial Synthesis Using Plasma Generation in Liquid. *J. Nanomater.* 2015, 2015, 123696.
- (37) Tan, K. S.; Cheong, K. Y. Advances of Ag, Cu, and Ag-Cu alloy nanoparticles synthesized via chemical reduction route. *J. Nanopart. Res.* 2013, 15 (4), 1537.
- (38) Hu, C. L.; Zhang, L.; Gong, J. L. Recent progress made in the mechanism comprehension and design of electrocatalysts for alkaline water splitting. *Energy Environ. Sci.* 2019, 12 (9), 2620–2645.
- (39) Lagadec, M. F.; Grimaud, A. Water electrolyzers with closed and open electrochemical systems. *Nat. Mater.* 2020, 19 (11), 1140–1150.
- (40) Engstfeld, A. K.; Maagaard, T.; Horch, S.; Chorkendorff, I.; Stephens, I. E. L. Polycrystalline and Single-Crystal Cu Electrodes: Influence of Experimental Conditions on the Electrochemical Properties in Alkaline Media. *Chem.—Eur. J.* 2018, 24 (67), 17743–17755.
- (41) Arán-Ais, R. M.; Scholten, F.; Kunze, S.; Rizo, R.; Roldan Cuenya, B. The role of in situ generated morphological motifs and Cu(i) species in C²⁺ product selectivity during CO₂ pulsed electroreduction. *Nat. Energy* 2020, 5 (4), 317–325.
- (42) Raaijman, S. J.; Arulmozhi, N.; da Silva, A. H. M.; Koper, M. T. M. Clean and Reproducible Voltammetry of Copper Single Crystals with Prominent Facet-Specific Features Using Induction Annealing. *J. Electrochem. Soc.* 2021, 168 (9), 096510.
- (43) Tiwari, A.; Heenen, H. H.; Bjørnlund, A. S.; Maagaard, T.; Cho, E.; Chorkendorff, I.; Kristoffersen, H. H.; Chan, K.; Horch, S. Fingerprint Voltammograms of Copper Single Crystals under Alkaline Conditions: A Fundamental Mechanistic Analysis. *J. Phys. Chem. Lett.* 2020, 11 (4), 1450–1455.
- (44) Feng, Y.; Li, Z.; Kang, S.; Cheng, C. Q.; He, B.; Guan, W.; Hu, X. Z.; Ji, L. P.; Yin, P. F.; Yang, J.; Dong, C. K.; Liu, H.; Cui, L.; Du, X. W. Mechanically processing copper plate into active catalyst for electrochemical hydrogen production. *Acta Mater.* 2022, 237, 118164.
- (45) Norskov, J. K.; Abild-Pedersen, F.; Studt, F.; Bligaard, T. Density functional theory in surface chemistry and catalysis. *Proc. Natl. Acad. Sci. U.S.A.* 2011, 108 (3), 937–943.
- (46) Heino, P.; Perondi, L.; Kaski, K.; Ristolainen, E. Stacking-fault energy of copper from molecular-dynamics simulations. *Phys. Rev. B* 1999, 60 (21), 14625–14631.



CAS BIOFINDER DISCOVERY PLATFORM™

BRIDGE BIOLOGY AND CHEMISTRY FOR FASTER ANSWERS

Analyze target relationships,
compound effects, and disease
pathways

Explore the platform

